Scientific Visualization, 2023, volume 15, number 4, pages 24 - 40, DOI: 10.26583/sv.15.4.03

RLaMs-Dehazing: Optimized Depth Map Improvement Single Colour Image Dehazing

Sangita Roy[1]

ECE Department, Narula Institute of Technology, Kolkata, India

[1] ORCID: 0000-0002-8898-0183, roysangita@gmail.com

Abstract

Visibility Degradation is a classical problem owing to the presence of Atmospheric Particulate Matter (APM). There are different image dehazing algorithms. Any one method cannot be relied upon as each haze condition is unique. An innovative algorithm has been proposed inverting the image formation atmospheric scattering model [2, 32]. The model has been improvised by one key factor. This is Regularized Lagrangian multiplier (RLaM) based Depth Map (DM) refinement. The algorithm has low time complexity which intrigues real-time efficient applications. Different state-of-the-art visibility algorithms have been studied and their subjective and objective performance evaluations have been evaluated. Extensive investigation shows remarkable improvement with the proposed algorithm. This method is equally applicable to different atmospheric conditions. Time complexity experimented with execution time and Big (O) for real-time effectiveness. Extensive experiment results show the potential of the proposed algorithm independent of the influence of atmospheric conditions and capturing devices adaptive to computer vision applications. Time complexity and quality output trade-off achieved with the removal of ringing artifacts efficiently.

Keywords: Airlight, Transmission estimation, APM, Ill-Posed Inverse Problem, Big (O).

1. Introduction

Rain, fog, vog, mist, fume, smog, hail, snow, etc. are considered as the source of APM. Researchers are fighting the challenge of the presence of APM which is due to unplanned civilization and technological advancements. Satellite images show that Asia and Africa and very few parts of American countries are the most polluted atmosphere deteriorating yearly. APM are both natural and manmade. APM is a mixture of solid and liquid droplets in a variety of sizes, Coarse APM as PM10-PM2.5 (micrometre diameter), finer as PM2.5, and ultrafine below PM0.1[1]. Computer vision (CV) encompasses object tracking, object recognition, surveillance, image enhancement, etc. A clear image is a fundamental requirement in CV applications. APM degrades the visibility of the received image. distance, airlight, transmission, and scattering coefficient influence image formation at the viewer point (i.e. may be considered camera) [2]. classical enhancement techniques, like, histogram equalization, image adjustment, and adaptive histogram equalization work well for the normal image enhancement process. These techniques fail in special cases of bad weather lowering the image visibility. Single image visibility restoration is the challenge of all other image visibility improvements as no ground truth or reference image could be found. Single image dehazing is one of the most sought-after single image visibility restoration techniques. Any outdoor clear image inherently possesses high contrast, airlight does not affect the richness of the image, pixel intensity is well distributed, and pixel over-saturation and under-saturation do not exist [22]. Contrary to that of hazy images are of low contrast and airlight makes images white. Most of the pixel intensities are very high i.e., under-saturated and flocked together. Over saturation occurs in one of the channels of the degraded image due to the illuminant of a strong colour cast, the response of the sensor/camera differently for different colour channels resulting in

achromatic image artifacts. Visibility Improvement is under the category of an ill-Posed Inverse Problem [1-16, 31-33]. The best image has to be evaluated from the attenuated received images. Inverting image formation optical model, a reconstructed image can be found as close to the original image depending on the applications. The paper is arranged as: section 2 consists of a Literature survey. The main contribution of the work has been identified in section 3. Proposed methods with mathematical modelling have been illustrated in Section 4. The result is described in section 5 with explains qualitative and quantitative analysis. Finally, section VI is for the Conclusion.

2. Background Theory and Associated Work

In some research work, DCP (dark channel prior) has been used which is a statistical prior on haze free images. This prior indicates that in a normal RGB image, 75% of pixels of any dark channel is zero where dark channel indicates the lowest intensities channel out of three RGB image channels. 90% pixels of that channel is below 25. However, the scenario drifts radically in case of degraded weather. That corresponds to the high intensity of the dark channel. It is due to atmospheric airlight which shifts the pixel's intensity to a very high value producing an almost white image. The method is efficient but takes a long time to reproduce. Therefore real time applications cannot be useful [4]. The work of R Tan is based on two observations, the contrast of image is compromised in the degraded image. Normal image has more contrast than that of hazy image. A degraded image has more airlight and it increases with distance. As a result distant part becomes smoother and invisible. The method is efficient as required a single image, but not applicable for real time [5]. The algorithm proposed by J P Tarel is fast and its complexity is a linear function with the number of image pixels for both colour and gray image. The algorithm is tuned by only four parameters, atmospheric veil inference, image restoration, smoothing, and tone mapping [6]. Research work of R Fattal based on haze estimation, and scatter light estimation. From that information, haze free image contrast has been recovered. It has been assumed that transmission and surface shading is locally uncorrelated. This simple statistical assumption reduces other complexity like surface albedo. The challenge of this method is to solve the pixels where no transmission is available. An implicit graphical model made it possible to extrapolate the solution of those pixels[7]. It is not a patch based prior contrary to previous methods. It is non-local prior. D Berman et. al. emphasised that degradation is not uniform. It is different for different pixels of the image and is controlled by the transmission coefficient. It has been proposed colours of haze free to be clustered and spread over the entire image. Whereas a hazy image forms a line of colours that was earlier clustered, called a haze line. It recovers the distance map. The algorithm is linear, faster, and deterministic, no training is required [8]. The author is working on visibility improvements. The works were DCP based vision improvements where the speed of the original algorithm was improved with reduced complexity and sky masking [9]. In [10] authors proposed three algorithms and revised DCP by gamma correction, contrast controller, sky masking and guided filtering. In [11, 12, and 13] authors emphasised on the objective evaluation of the DCP method and mathematical modeling of image formation. DCP is basically patch based or local prior. Patch size in [4] was 15x15, omega was 0.95. These two parameters play a significant role. This has been shown [14]. DCP with sky masking is a useful algorithm. But the value of optimum value is difficult to find out. It is evaluated manually. In [5] this difficulty has been recovered by using Cuckoo Search Algorithm. The resultant image using CSA removes the artifacts of sky reflection very well. Visibility Improvement is a classical Inverse problem. Haze is always associated with blurring. Here both have been treated and removed [3-16].

3. Main Contribution of the paper

As discussed above single image colour dehazing is a challenge and complex in nature. In this work low complexity depth map non-linear noise removal model has been estimated. Im-

age degradation optical model with refined transmission via RLaMs depth map estimation produces the resulting reconstructed output. Apart from that haziness factor k has been evaluated automatically depending on the spread of intensity in the depth map [33].

3.1 Regularized Lagrange Multiplier (RLaM) and Point Spread Function(PSF)

Blur is an integral part of any degraded image. It comes along with nonlinear noise. The degrading system prior model has to be reconstructed from blurred or degraded images. Linear filters like Wiener, Least square filter, and nonlinear filters like Lucy Richardson filter have also been studied. RLaMs have been applied to remove blur which has been compared to classical methods using parametric assessment of PSNR and time consumed [24, 25]. RLaMs are effective and important in computer graphics applications as it is non-iterative, fast, and bypass the problem of parameterizing system's degree of freedom. Finally, it has computational complexity O(n).[28].These advantages of LaMs have been adapted in this research work. The PSF is a quantity to determine the power of an optical system. Better resolution may be achieved by narrowing the PSF. It is the spread of a point source of light as it passes through a system. Ideally, a point source in space is defined by the delta function infinite spectrum in special frequency kx, ky. PSF of an image forming optical system is resolved by the parameter of an optical system and the distance or depth of the object to be imaged [29]. Figure 3 shows PSF(Point Spread Function) with Gaussian kernel 3x3 and standard deviation 10, noise variance 0.1. Twelve different outdoor natural degraded images have been recovered with Regularized Lagrange Multiplier with the above PSF. It is often encountered in engineering and science applications the discretization of linear ill-conditioned problems. This leads to large ill-conditioned linear systems with right hand side corrupted by noise [27]. The solution of this kind of linear system needs the solution of a minimizing problem which is dependent on the estimation of the variance of the noise. This approach is well-known as regularization. Lagrangian is a technique to solve this type of Noise Constrained Regularization problem.

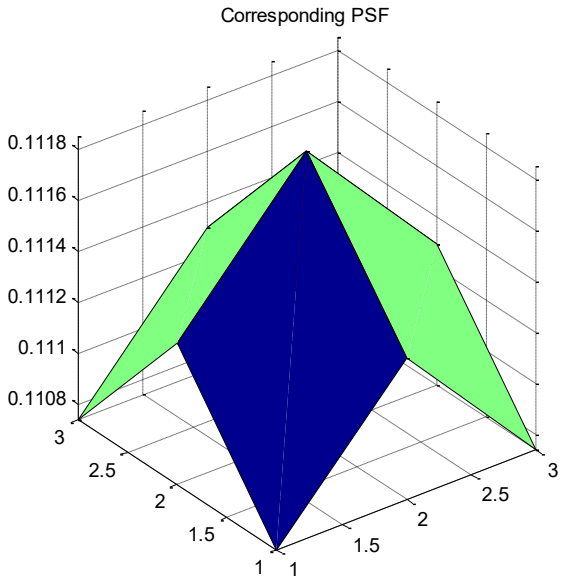

Fig. 1 Point Spread Function used with Gaussian kernel 3x3 and standard deviation 10, noise variance 0.1.

3.2 Image Formation Process

Initially image restoration method is considered under the category of linear spatially invariant restored filters. Blurring function is considered as point spread function (PSF) or convolution kernel h (n_1, h_2). Statistical properties (mean, correlation) of the original image are assumed to be non-changeable spatially. Under these conditions image formation mathematical model is formulated. Here f (n_1, n2) is the ideal spatially discrete image with no blur or noise. The received image is displayed as

$$g(n_1, n_2) = h(n_1, n_2) * f(n_1, n_2) = \\ = \sum_{k_1=0}^{N-1} \sum_{K_2=0}^{M-1} h(k_1, k_2)\, f(n_1 - k_1, n_2 - k_2) \qquad 3.2.1$$

The above equation can be rewritten in matrix form.$F \in \mathbb{R}^{r\times n}$ is the matrix form of original image.$G \in \mathbb{R}^{r\times m}$ is the corresponding degraded image. $f_{i,j}$ is the pixel elements i=1.....r and j=1.....n. $H \in \mathbb{R}^{m\times n}$ is the degradation matrix. Each row of matrix are related by

$$g = Hf, g \in \mathbb{R}^m, f \in \mathbb{R}^n, H \in \mathbb{R}^{m\times n} \qquad 3.2.2$$

Where $f = f_i^T \; and \; f_i$ represents ith row of the original image F. Similarly $g = g_i^T \; and \; g_i$ represents ith row of the degraded image G. The process is repeated for each row of the matrix and develops an unknown system of m simultaneous equations with n=m+l-1. It is now easy to evaluate PSF which is assumed to be spatially invariant, and the degradation matrix H with zero boundary conditions. It is assumed that the length of blur be l in pixels which is also known as degradation index and an integer. Degradation index 'l' is very difficult to find and has to be approximated from the degraded image. Degradation index 'l' can be recovered by two methods i) one dimensional cepstral method, ii) two dimensional cepstral method. It is now important to find i^{th} row of the blurred image from the i^{th} row of the original image using the eq 3.2.2.

$$\begin{bmatrix} g_{i,1} \\ g_{i,2} \\ g_{i,3} \\ \cdot \\ \cdot \\ \cdot \\ g_{i,m} \end{bmatrix} = \begin{bmatrix} h_1 & \cdots & h_l & 0 & 0 & 0 & 0 \\ 0 & h_1 & \ldots & h_l & 0 & 0 & 0 \\ 0 & 0 & h_1 & \ldots & h_l & 0 & 0 \\ 0 & 0 & 0 & h_1 & \ldots & h_l & 0 \\ 0 & 0 & 0 & 0 & h_1 & \ldots & h_l \end{bmatrix} \begin{bmatrix} f_{i,1} \\ f_{i,2} \\ f_{i,3} \\ . \\ . \\ . \\ f_{i,m} \end{bmatrix} \qquad 3.2.3$$

Where $h_i = \frac{1}{l} \; for \; i = 1, \ldots \ldots . l, h_i \; is \; the \; element \; of \; H \; matrix$. The main objective is to retrieve original image from degraded image G and priori knowledge of degraded phenomena matrix H. The matrix $\in \mathbb{C}^{r\times m}$, blurred image, can be written mathematically

$$g_{i,j} = \frac{1}{l} \sum_{k=0}^{l-1} f_{i,j+k} \; , i = 1 \ldots r, j = 1 \ldots m \qquad 3.2.4$$

Now eq 3.2.4 can be rewritten as

$$G = (HF^T)^T = FH^T, G \in \mathbb{R}^{r\times m}, H \in \mathbb{R}^{m\times n}, F \in \mathbb{R}^{r\times n} \qquad 3.2.5$$

It is clear that there are infinite of exact solutions for f satisfying the eq 3.2.2 and 3.2.5. Out of them sharpest restored matrix is essential. The vertical blur matrix is given by

$$G = HF, G \in \mathbb{R}^{m\times n}, H \in \mathbb{R}^{m\times r}, F \in \mathbb{R}^{r\times n}, r = m + l - 1 \qquad 3.2.6$$

Now this is assumed that blurring of rows is independent of blurring of columns in image. Consequently there exists two matrices H_c and H_r. In such a scenario these can be expressed as

$$G = H_c F_r^T, G \in \mathbb{R}^{m1\times m2}, H_c \in \mathbb{R}^{m1\times r}, F \in \mathbb{R}^{r\times n}, H_r \in \mathbb{R}^{m2\times n} \qquad 3.2.7$$

Where n=m_2+l_1-1, r=m_1+l_2-1, l_1 is linear horizontal blur in pixel, and l_2 is linear vertical blur in pixel.

3.3 Image Recovery by Regularized Lagrange Multiplier

In this section an excellent method has been reviewed known as Lagrange Multiplier (LM). This is a linear blur model. The main purpose of the LM is to remove linear blur and recover original image as optimum as possible [fumi]. It is assumed that blur length is integer number of pixels and resolution of the recovered image is very high. From eq 3.2.2 $\boldsymbol{g=Hf}$, where $\boldsymbol{f}$ is the first '$\boldsymbol{m}$' components of '$\boldsymbol{f}$' which has minimum distance from measured data, $\|\tilde{\boldsymbol{f}} - \boldsymbol{g}\| \rightarrow \boldsymbol{min}$ $\boldsymbol{3.2.1}$. Now it is assumed that $\tilde{\boldsymbol{f}} = \boldsymbol{Pf}$. $\boldsymbol{P}$ is a $\boldsymbol{mxn}$ matrix to project $\boldsymbol{f}$ using the backing of $\boldsymbol{g}$.

$$P = [I_m | O] \tag{3.3.1}$$

Where $\boldsymbol{I_m}$ denotes identity matrix of size $\boldsymbol{mxm}$ and $\boldsymbol{O}$ signifies $\boldsymbol{mx(l-1)}$ *null matrix.* Eq 3.2.1, original optimization problem, is redefined as

$$\min_f \|Pf - g\| \tag{3.3.2}$$

While subject to constrain $\|Hf - g\|^2 = 0$ 3.2.4. Therefore eq 3.2.3, and 3.2.4 are together a constrain optimization problem. Using LMs, an alternate optimization problem without constrain can be modelled.

$$V(f) = \lambda\|Hf - g\|^2 + \|Pf - g\|^2 \rightarrow \min \tag{3.3.3}$$

λ is known as Lagrange multiplier. Equation 3.2.5 is strictly convex and low semi continuous with respect to weak-star bounded space topology [24-26]. Now partial derivative of V with respect to unknown f for very high λ:

$$\frac{\delta}{\delta f}V(f) = 2\lambda H^T(Hf - g) - 2P^T(Pf - g) = 0 \tag{3.3.4}$$

$$\check{f} = (\lambda HH^T + P^TP)^{-1}(\lambda H + P)^T g \tag{3.3.5}$$

The solution of eq 3.2.7 in the matrix form is:

$$\check{F} = G(\lambda H + P)((\lambda HH^T + P^TP)^{-1})^T \tag{3.3.6}$$

The eq 3.2.7 interprets the solution of recovered image in the horizontal blurring condition. In case of vertical blurring scenario equation 3.2.6 and 3.2.7 will be helpful.

$$\check{F} = (\lambda H^TH + P^TP)^{-1}(\lambda H + P)^T G \tag{3.3.7}$$

Now for a two dimensional separable blurring processes the recovered image is:

$$\check{F} = (\lambda H^TH + P^TP)^{-1}(\lambda H + P)^T G\ (\lambda H + P)((\lambda HH^T + P^TP)^{-1})^T \tag{3.3.8}$$

3.4 Time Complexity

There are numerous algorithms to solve a specific problem. Out of several algorithms, one of them has to be chosen. There are also several criteria to fit one algorithm for a problem. **Efficiency** criteria will meet and fit for algorithmic fitness selection in computational computing. Efficiency encompasses three criteria: i) time efficiency, ii) space efficiency, and iii) Development efficiency [30]. Time complexity in terms of execution time and big oh notation has been experimented and one way of classifying and comparing algorithms.

4. Single Colour Image Restoration

Using the above described techniques a novel algorithm has been effectively designed to remove atmospheric turbulence as well as system degradation on single colour image. Total algorithm with their detail mathematical modelling is given below in the corresponding subsections.

4.1 Proposed Methodology

In this paper, a novel algorithm based on inverting H Koschmieder and E J McCartney image formation optical model [2,32] has been presented. Transmission is refined through **Lagrange Multiplier**-based depth map estimation and followed by YCbCr correction as shown in Fig. 2 [24-29]. They are elaborated below.

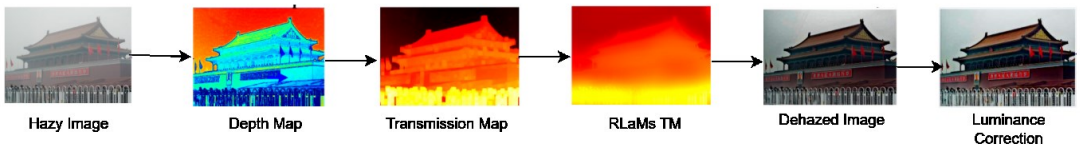

Figure 2. Block Diagram of the RLaMs (Proposed Model).

	Algorithm 1: RLaMs	
	Input Hazy Image:I	Computational Complexity
Step I	Average of minimum of three channels as I_{min}	O(n)
Step II	Average of maximum value of three channels as I_{max}	O(n)
Step III	Haziness factor, k =I_{min} / I_{max} Eq. (4.4.1)	O(n)
Step IV	Airlight Estimation	O(n)
Step V	Estimation of minimum intensity channel	O(n)
Step VI	Refinement / noise removal of minimum intensity channel by Regularized Lagrange Multiplier Technique (used as Depth Estimation) [28]	O(n)
Step VII	Transmission Estimation from step VII Eq. (4.3.4)	O(n)
Step VIII	Recovery of Dehazed image with image degradation optical model [2, 38, 39]. Eq.(4.6.1)	O(n)
Step IX	YCbCr correction	O(n)
Step X	Evaluation of contrast,k, β and dmax of the Dehazed Image	O(n)

The image formation model, also known as airlight scattering model, was proposed by H Koschmieder, and E J McCartney [2, 32] and represented as an ill-posed problem in equation (4.1.1).

I(x): the hazy image at a point x,
J(x): the haze-free image,
t(x): the transmission map,
A: atmospheric light,
β: atmospheric extinction coefficient,
d: distance between the original image and hazy image or depth of scene.

Here ***I, J,*** and ***A*** are 3-D RGB image arrays. Six variables are shown above. Only ***I***, the hazy image, is known.

J has to be developed from ***I, t, A, β***. Estimation of ***A, t*** and **β** are responsible for good quality dehazed image.

$$I(x) = J(x)t(x) + A\big(1 - t(x)\big) \quad 4.1.1.$$

$$t = e^{-\beta d} \quad 4.1.2$$

4.2 LMs-based Improved Depth Information estimation

Noise is an integral part of an imaging system. The transmission map, a 2D image array, is severely captured by noise. The dehazed image is restored by minimizing **TM**. TM is obtained by inverting DM with proper selection of haziness factor [33]. Transmission map is solely associated with depth information and inaccurate estimation leads to the halo effect leading to a high computational cost problem [3-16,33] and is associated as an understanding

of geometric relationships in a scene. Single image DM estimation is far harder than multiple images and to simplify patch-based dark channel [4], DM is estimated as the minimum of three channels. Random noise on the minimum channel is eliminated by RLaMs mentioned earlier in section 3.1.

$$I_{cmin}(x) = \left(\min_{c\in\{r,g,b\}}(I^c(x)\right) \quad 4.2.1$$

I^c : indicate individual channels of RGB image,
Icmin: minimum of three channels I^c (noisy),
IcminLMs : RLaMs Icmin (noisefree)
Noisy Icmin is made noiseless through Lagrange Multiplier and is considered as refined normalized DM.

$$I_{cminLMs}(x) = RLMs(I_{cmin}(x)) \quad 4.2.2$$

Complimenting equation (4.2.2) will produce low complexity edge preserved smooth maximum intensity. This maximum intensity channel will be treated as the **TM** t(x) [4, 17-29]. Whereas this proposed concept is computationally simple and easy to implement.

4.3 Transmission estimation using refined Depth map

Intensity from any far point pixel in the minimum intensity channel may be zero and totally faded away with distance and represented as atmospheric light ***A*** [0 1] as in equation (4.1.1). This can be rewritten below.

$$I_{cmin}(x) = A(1 - t(x)) \quad 4.3.1$$

In marginal case, equation 4.3.1 can be refined with atmospheric light ***A*** as one for the far end point as below.

$$I_{cmin}(x) = 1 - t(x) \quad 4.3.2$$

Another improvement needed as $\boldsymbol{I_{cmin}}$ is noisy and after ***RLaMs*** based refinement on depth map estimation according to equation (4.2.2) transmission equation will be rewritten as F

$$I_{cminlms} = LMS(I_{cmin}) \quad 4.3.3$$

$$t_{new}(x) = 1 - I_{cminLMs} \quad 4.3.4$$

Now after getting refined transmission map for individual image, $t_{new}(x)$ will not be the same for each image, as individual scenario is different. Therefore additional factor, *haziness factor* k, is required to be introduced.

$$t_{new}(x) = 1 - kI_{cminLMs} \quad 4.3.5$$

K is a proportionality constant for aerial perspective respectively. Zero indicates clear visibility like clear day scene, whereas one indicates absolutely no visibility like thick fog [4, 7, 33].

4.4 Automated Haziness Factor Estimation

$$k = \frac{I_{cmin}}{I_{cmax}} \; 4.4.1 \quad 4.4.1$$

It has already been stated that k, haziness factor, indicates the amount of haze present in the image of interest. So far this is calculated manually by visual inspection of the amount of haze. But for real time applications this cannot be implemented. The author has already worked with this [31, 33]. Here it is considered that haziness factor k is the ratio of the average of the minimum intensity channel to the average of the maximum intensity channel. This concept works well for real time adaptive visibility improvement.

4.5 Atmospheric Light Estimation

Image formation optical model indicates that transmission decays exponentially with distance in Eq. (4.1.1), (4.1.2). In the end, the far end or background becomes whitish and technically as equal to A, atmospheric light [2, 4, 32, 33] and distant pixels are maximum bright due to haze. it has been proposed atmospheric light to be maximum bright pixels in an image.

For more robust estimation, atmospheric light A has been considered to be the top 0.1% bright pixels of each channel.

An example has been explained in Fig. 5. It shows the degraded image, its depth map and transmission map, recovered image, its depth map, and transmission map by the proposed RLaMs-Dehazing algorithm. It is evident not only from the recovered image but also from the recovered depth map and transmission map that the proposed algorithm works well and serves its purpose of cleaning the image.

4.6 Scene radiance recovery using scattering image formation optical model

The main objective of the work is to retrieve the original hazefree or scene radiance image. Therefore from equation 4.1.1 scene radiance can be recovered. This is shown below.

$$J(x) = \frac{I(x)}{t_{new}(x)} - \frac{A\big(1 - t(x)\big)}{t_{new}(x)} \qquad 4.6.1$$

4.7 YCbCr correction of the scene radiance image

Y is luma or intensity or achromatic colour channel component of any colour image. Cb and Cr are blue difference and red difference respectively. Luminance channel Y is independent of colour information, that is why YCbCr format performs better.By controlling y channel intensity keeping Cb and Cr channels unaffected radiance image brightness may be enhanced, so that gloomy radiance image may be look brighter. This is shown by an example in Fig. 3. Radiance dehazed image visibility may be enhanced by this YCbCr correction.

Fig. 3. Left: Hazy input, Middle: Scene Radiance, Right: YCbCr correction

5. Experimental Result

In this section, the performance of the RLaMs dehazing technique is examined from various aspects. At first, ten sample hazy images from the O-Haze dataset were examined with the RLaMs technique. GT, DM, refined DM, TM, refined TM, and RLaMs output were tested qualitatively and quantitatively.

5.1 Performance of the RLaMs

Haze is not uniform and changes its density in each situation. The popularity of any dehazing algorithm depends on its visibility improvement qualitatively and quantitatively [4-16, 30-35]. Ten hazy images from the O-Haze dataset were selected randomly to investigate the effectiveness of the RLaMs. The results in Fig 4 show those randomly picked images along with their DM, TM, refined DM, refined TM, and dehazed outputs. The figure reveals the essential details along with compatible DM, and TM texture for human perception cues. Artifactfree, balanced coloured, and clear outputs are obtained. The sky and clouds look natural. The different depths and haze of those images are well rectified.

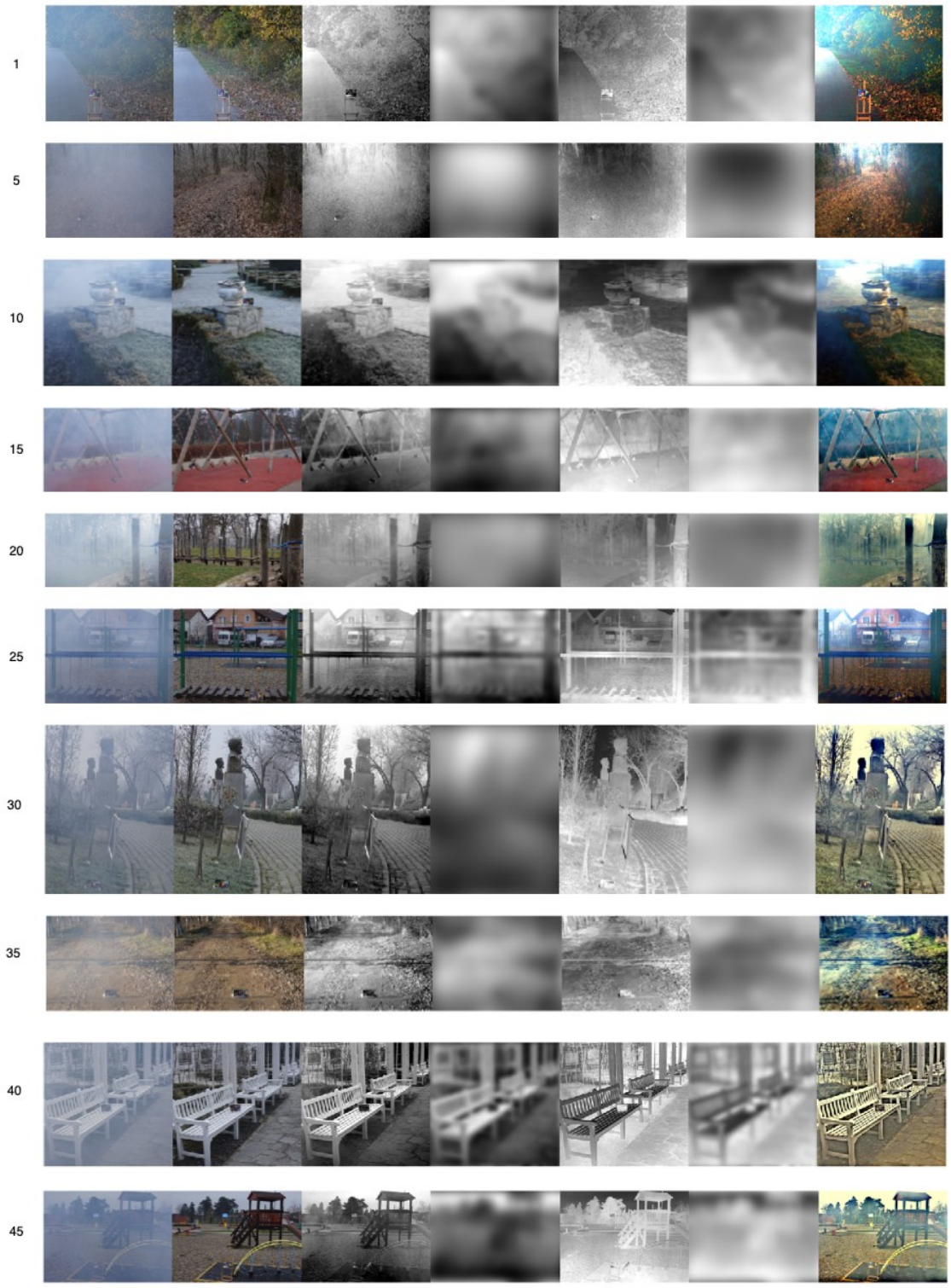

Fig. 4. Performance of the proposed RLaMs dehazing method, **Left:-Right:** Dense Input hazy Image, GT, DM, **Refined DM,** TM, Refined TM, RLaMs. 10 images O-Haze dataset [34].

5.2 Qualitative /subjective evaluation

To validate the proposed algorithm, two types of image datasets were selected, real world and synthetic.

a) Relative Study on Real world images, Ref [36]

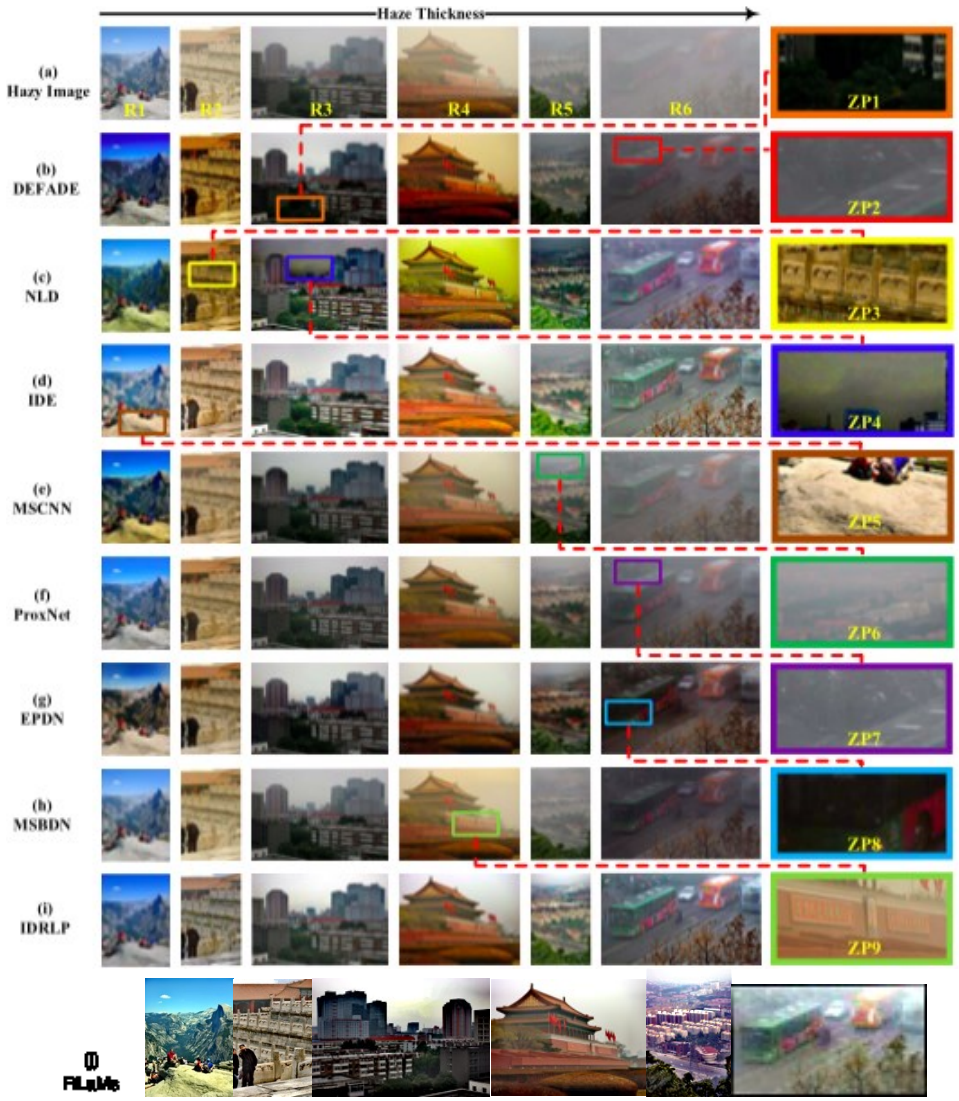

Fig. 5. Subjective performance of the state-of-the-art techniques and RLaMs using Real world images [34].

To verify the power of the RLaMs, eight state-of-the-art techniques (DEFADE [37], NLD [38], IDE [39], MSCNN [40], ProxNet [41], EPDN [42], MSBDN [43], and IDRLP [35]) were experimented with the RLaMs. Images from the real-world varied haze thickness dataset in ref [36] are picked here. The subjective results are shown in Fig. 5. Fig. 5(b-i) generates clear output applicable to computer vision. Fig. 5(j) produces exceptionally clear and detailed textures in comparison to Fig. 5(b-i). Fig. 6(ZP1-ZP9) shows artifacts and shortcomings in [37-43, 35] failing to handle haze, darkness, sky region, and colour over saturation. In Fig. 5(j), most of the shortcomings in Fig. 5 (a-i) are circumvented.

b) Relative Study on Synthetic images with Haze-free GT as Refs [44, 34, 45]

Single image dehazing is the most difficult of all image restoration problems. Haze-free GT is an important criterion to validate any image restoration algorithm. GT haze-free images from References SOTs, I-Haze, and O-Haze datasets [44, 34, 45] have been used in Fig. 6 for comparable analysis of RLaMs with eight state-of-the-art techniques (DEFADE, NLD, IDE, MSCNN, ProxNet, EPDN, MSBDN, and IDRLP) as [37-43, 35] respectively. Six images, two from each dataset, have been selected sporadically in Fig. 6. As in Fig. 6, RLaMs generate clear textured outputs befitting for CV applications. In analytical study, comparable subjective results were observed as in Fig. 5. High resemblance is obtained between Fig. 6(b) as GT and 6(k) as RLaMs.

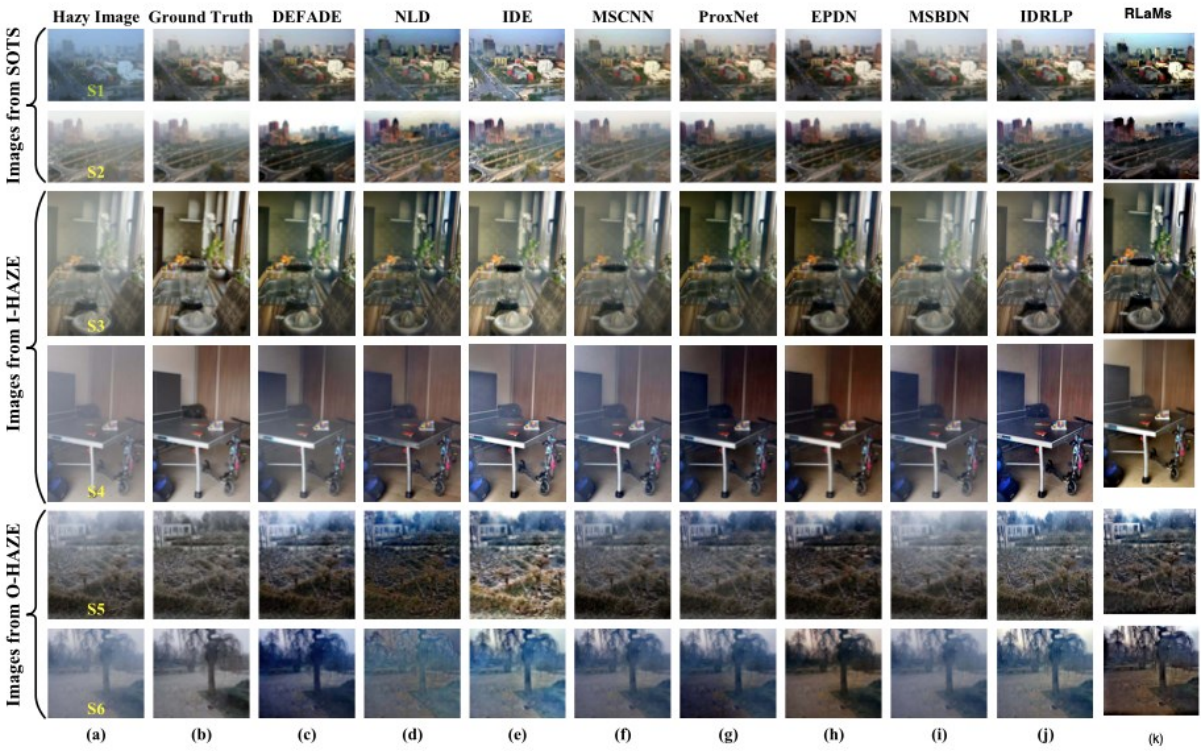

Fig. 6. Qualitative comparison between the proposed RLaMs and state-of-the-art techniques on six synthesis images.

5.3 Objective Evaluation

The quantitative assessment using PSNR and SSIM of the proposed model is summarized in Table I. Progressive results with the RLaMs showed its effectiveness in different kinds of haze removal. In six images of three different data sets in Fig. 6, the RLaMs performs the best of eight state-of-the-art methods with the average PSNR/SSIM values of the six images. Comparable clear results with RLaMs and GT are found. The ranking of the nine techniques is also shown in Table I along with their ranking. The ranking clarifies the effectiveness of the RLaMs-Dehazing technique(Ranking: 2,1,4,1,1,1,3,1,1,1,1, and 1). It is evident that the proposed technique is fit quantitatively. Table II shows the ranking list. The RLaMs_Dehazing tops the list with a considerable margin.

TABLE I

PSNR AND SSIM Analysis of DEFADE, NLD, IDE, MSCNN, ProxNet, EPDN, MSBDN, IDRLP and RLaMs_Dehazing in Fig. 6.

Metric	Image	DEFADE	NLD.	IDE	MSCNN.	ProxNet	EPDN.	MSBDN	IDRLP	RLaMs.
PSNR/ /SSIM	S1	18.0934(6)/ 0.8561(4)	15.5077(9)/ 0.6704(9)	16.3054(8)/ 0.7481(7)	16.8744(7)/ 0.7192(8)	20.1954(4)/ 0.8552(5)	19.4554(5)/ 0.8324(6)	31.1525(1)/ 0.9485(2)	23.9166(3)/ 0.9306(3)	24.1519(2)/ 0.9738(1)
	S2	24.7166(2)/ 0.8954(4)	15.4555(9)/ 0.6374(9)	15.9776(8)/ 0.7055(8)	18.3954(5)/ 0.8599(6)	18.1939(7)/ 0.8654(5)	18.2712(6)/ 0.8005(7)	28.3496(1)/ 0.9349(2)	24.6631(3)/ 0.9246(3)	23.4499(4)/ 0.9674(1)
	S3	18.0567(5)/ 0.6988(6)	15.7747(8)/ 0.7117(5)	18.2169(4)/ 0.6864(8)	18.2825(3)/ 0.7279(4)	17.3509(6)/ 0.7401(3)	14.9668(9)/ 0.6628(9)	16.9563(7)/ 0.6978(7)	20.0093(2)/ 0.7597(2)	20.8031(1)/ 0.9363(1)
	S4	20.0381(4)/ 0.6711(6)	15.0614(8)/ 0.7211(3)	18.7158(5)/ 0.6714(5)	17.3144(6)/ 0.4239(8)	15.5291(7)/ 0.4136(9)	13.8245(9)/ 0.6576(7)	21.4035(2)/ 0.6776(4)	21.8769(1)/ 0.7421(2)	20.9186(3)/ 0.9440(1)
	S5	17.1711(6)/ 0.6398(7)	16.8367(8)/ 0.6379(8)	14.4937(9)/ 0.6364(9)	20.7825(4)/ 0.7569(5)	22.2129(3)/ 0.8189(3)	17.0468(7)/ 0.6786(6)	18.5818(5)/ 0.7957(4)	22.7703(2)/ 0.8606(2)	25.7597(1)/ 0.9862(1)
	S6	15.0914(8)/ 0.5838(8)	16.1412(7)/ 0.7072(3)	17.2408(4)/ 0.6158(6)	16.9906(5) 0.6507(5)	14.3009(9)/ 0.6001(7)	16.2403(6)/ 0.5684(9)	21.0918(3)/ 0.6826(4)	21.4311(2)/ 0.7563(2)	21.6392(1)/ 0.9554(1)

TABLE II

PSNR/SSIM	DEFADE	NLD.	IDE	MSCNN.	ProxNet	EPDN.	MSBDN	IDRLP	RLaMs.
Ranking	31/35	49/37	38/41	30/ 36	36/32	42/44	19/23	13/14	12/06

In Table III, performance analysis was conducted on SOTs, I-Haze, and O-Haze Datasets in Fig. 6. The average PSNR/ SSIM of those images is listed in groups in comparison with the eight above-mentioned benchmark algorithms and the RLaMs_Dehazed method along with their ranking. In Table III, the ranking of the RLaMs again shows its superiority over the other eight methods.

TABLE III

Performance as Average PSNR/ SSIM of DEFADE, NLD, IDE, MSCNN, ProxNet, EPDN, MSBDN, IDRLP and RLaMs_Dehazing with SOTS. I-Haze, and O-Haze Datasets:

Image	DEFADE Matlab CPU	NLD. Matlab CPU	IDE Matlab CPU	MSCNN. Matlab CPU	ProxNet Matlab CPU	EPDN. Pytorch CPU/GPU	MSBDN Pytorch CPU/GPU	IDRLP Matlab CPU	RLaMs. Matlab CPU
SOTs	16.9045(9)/ 0.7498(9)	18.5907(7)/ 0.8080(5)	19.2062(6)/ 0.7985(6)	16.9549(8)/ 0.7592(8)	20.7005(5)/ 0.8458(4)	22.9536(4)/ 0.7785(7)	33.666(1)/ 0.9876(1)	23.568(3)/ 0.9383(3)	24.2618(2)/ 0.9828(2)
I-Haze	15.9535(5)/ 0.7500(5)	14.5387(8)/ 0.7197(7)	15.9172(6)/ 0.7204(6)	16.5441(4)/ 0.7783(3)	14.2560(9)/ 0.7114(9)	15.4013(7)/ 0.7192(8)	16.699(3)/ 0.7658(4)	17.355(2)/ 0.7896(2)	23.2142(1)/ 0.9825(1)
O-Haze	15.3412(7)/ 0.6049(9)	13.3776(9)/ 0.6054(8)	14.2990(8)/ 0.6325(7)	16.6224(4)/ 0.6917(3)	16.1567(6)/ 0.6582(6)	16.8574(3)/ 0.6793(4)	16.4633(5)/ 0.6596(5)	16.9492(2)/ 0.6990(2)	22.2337(1)/ 0.9577(1)

5.4 Computational Complexity

Apart from subjective and objective evaluation, computational complexity plays an important role w.r.t any algorithmic performance in computer vision applications [23]. As shown in Algorithm 1, ten steps have O(n) complexity each. Thus, the overall complexity of Algorithm 1 is O(n). This indicates that the algorithm is a linear relationship with the size of the image (MXN). The time complexity of the eight state-of-the-art models and RLaMs tested with the R1, R2, R3, and R4 in Fig. 5 is summerized in Table IV. The results of the different resolutions of those images are listed in Table IV. The RLaMs-Dehazing proves its fastness in all types of images defeating the other contestants.

5.5 Effect of Lagrange Multiplier

Five images from O-Haze, I-Haze, and SOTs (11,21,11,21,1410.11) were randomly chosen with its GT, Hazy and RLaMs-Dehazing in Fig. 7. In Fig. 8, Cropped version of Fig. 7 shows the effectiveness of RLaMs with seven Lagrange Multiplier values in Table V. No artifacts was found. Moreover, it also verified the range of RLaMs [0.312,1.0953] for effective results.

Fig. 7. First Row: Hazy Images(O_Haze(11,21), I_haze(11,21), SOTs); Second Row: GT; Third Row: RLaMs Dehaze Images

TABLE IV
Processing Time (seconds) of DEFADE, NLD, IDE, MSCNN, ProxNet, EPDN, MSBDN, and IDRLP and RLaMs_Dehazing with R1, R2, R3, and R4 in Fig. 6

Image	Resolution	DEFADE Matlab CPU	NLD. Matlab CPU	IDE Matlab CPU	MSCNN. Matlab CPU	ProxNet Matlab CPU	EPDN. Pytorch CPU/GPU	MSBDN Pytorch CPU/GPU	IDRLP Matlab CPU	RLaMs. Matlab CPU
R1	384x256	4.6329	0.3469	0.2688	0.5463	0.9948	1.1713/0.9329	1.2926/0.2448	0.2236	**0.121**
	768x512	15.1255	1.1053	0.4263	2.2241	1.9373	1.8007/1.1131	4.7321/0.4448	0.371	**0.214**
	1536x1024	61.6518	4.4785	1.1508	8.2105	6.5916	4.2879/1.7100	18.1626/1.2097	0.8961	**0.605**
	2304x1536	163.5108	10.2591	2.3662	17.9908	12.9918	8.7772/3.0749	40.4204/2.6119	1.7923	**1.228**
	3072x2048	559.9355	19.0473	3.9435	34.6651	25.5768	17.7368/4.9513	72.2998/___	2.831	**2.213**
	3840x2560	____	33.2637	5.8695	90.6309	39.2949	47.2435/7.0067	112.2309/__	3.9	**3.4**
	4608x3072	____	57.7944	8.4727	206.419	84.6179	63.8665/12.3614	167.119/___	5.7305	**5.15**
R2	200x300	2.5092	0.2579	0.2248	0.3243	0.8137	1.1713/0.9638	0.7490/0.2004	0.1451	**0.127**
	400x600	8.8374	0.6739	0.3484	1.3773	1.3792	1.4705/ 1.0228	2.6342/0.3321	0.214	**0.18**
	800x1200	35.2334	2.4448	0.8235	4.7191	3.4135	3.1147/ 1.5045	9.9256/0.9720	0.5195	**0.425**
	1200x1800	90.036	5.5109	1.5774	10.0857	6.7086	5.7403/ 2.3402	22.9646/ 2.0259	0.9633	**0.823**
	1600x2400	193.4217	10.3289	2.6529	19.1907	11.96	9.6121/ 3.5019	42.1790/ 3.2931	1.5216	**1.433**
	2000x3000	526.5829	16.6927	3.9094	32.8263	18.0075	14.9175/5.0843	65.6165/___	2.2902	**2.151**
	2400x3600	____	27.4001	5.3295	81.2978	26.7281	33.8060/ 6.7136	93.8091/___	3.2611	**2.222**
R3	300x200	2.651	0.2406	0.2502	0.3322	0.8665	1.1479/0.908	0.6960/0.2934	0.11504	**0.11**
	600x400	8.763	0.623	0.3516	1.2124	1.3329	1.5465/1.0750	2.840/0.3559	0.2206	**0.177**
	1200x800	35.7391	2.4185	0.7764	4.3774	3.1446	2.9682/1.4781	10.2122/0.9100	0.5188	**0.382**
	1800x1200	90.0897	5.3842	1.5378	9.496	6.4491	5.6248/2.2185	23.6761/1.7473	0.9069	**0.729**
	2400x1600	208.5686	9.9252	2.5362	18.4079	11.3481	9.3365/3.2394	41.9415/2.8769	1.5689	**1.235**
	3000x2000	530.3279	16.1275	3.7725	32.3711	17.5248	14.4812/4.5555	65.7886/___	2.3535	**1.894**
	3600x2400	____	26.4553	5.1334	82.8085	25.9558	34.0248/6.0548	94.9250/___	3.2204	**2.793**
R4	300x225	2.913	0.2635	0.2554	0.3433	0.9318	1.1872/0.9390	0.85440/0.2144	0.1625	**0.15**
	600x450	10.0109	0.6838	0.3547	1.2981	1.5903	1.5857/1.0641	2.9939/0.3727	0.2584	**0.177**
	1200x900	43.1763	2.6631	0.8545	4.7528	4.1895	3.2911/1.5713	11.5650/0.9544	0.5496	**0.408**
	1800x1350	119.5967	5.8451	1.6408	10.5	8.6642	6.4546/2.4704	26.8620/1.9026	0.9969	**0.816**
	2400x1800	236.5677	11.6924	2.707	19.2239	14.8764	10.4873/3.4665	47.7061/3.1996	1.6409	**1.365**
	3000x2250	750.8358	18.5929	4.243	42.454	23.8864	17.3574/4.9715	75.7184/___	2.5623	**2.194**
	3600x2700	___	31.5513	5.724	132.9783	34.5697	44.6102/6.8000	103.3466/___	3.5414	**3.07**

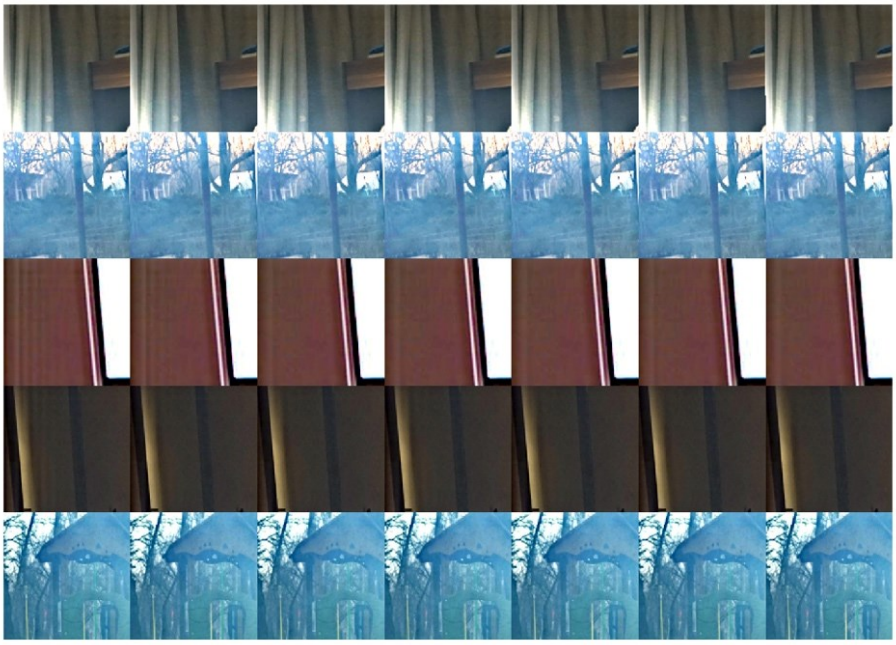

Fig. 8. Crop version of Fig. 8. with seven Lagrange Multiplier values; O-Haze(11,21), I-Haze(11,21, SOTs (1410.11)

TABLE V
Lagrange Multiplier used in the above five images with seven Lagrange Multiplier values

Lagrange Multiplier	**1.0953**	**0.3916**	**0.1563**	**0.1322**	**0.1037**	**0.0698**	**0.0312**

6. Conclusion

Particles suspended in the air cause hindrance in the path of light travel. This effect produces serious artifacts and degradation in the image formation process in the digital image reconstruction system with poor or no visibility. To improve visibility in the digital image, a low complexity, fast, robust visibility improvement is presented. The Lagrange-based regularized method is incorporated to refine TM through DM which improves transmission followed by inverting image formation optical model; finally, YCbCr correction enhances the results. In this paper, a novel regularized Lagrange Multiplier-based image visibility improvement technique RLaMs-Dehaze is presented. TM is purified through clean DM by the RLaMs optimization technique. These RLaMs are powerful, robust and low complexity in time; especially linear in time with the size of the image under investigation. Experiments on a diverse set of real-world images, and synthetic haze datasets demonstrate the preeminence of RLaMs-Dehaze over benchmark methods. Eight benchmark methods were selected for this experiment and excellent results were achieved for the superiority of the RLaMs-Dehazing qualitatively and quantitatively.

Drawback

RLaMs method produces more visibility than existing procedures. More modification possibilities are there to improve the algorithms depending on transmission maps TM and atmospheric light estimations (A). The weather condition of each image is unique. Therefore no one method can be claimed to optimally solve the problem equally.

Conflict of interest*:* No conflict of interest.

Highlight of the RLaMs Dehazing: RLaMs DM refinement, followed by TM correction. Inverting optical image formation model. YcbCr correction.

Acronym: DM: Depth Map; TM: Transmission Map; GT: Ground Truth; CV: Computer Vision

Resource:

a) Software: Matlab2014a is used as software for experiments.

b) Hardware: Intel core i3, 3110M CPU @ 2.40 GHz, 4.0 GB RAM, Intel HD Graphics 4000, 6 years old has been used for the research.

c) Dataset: SOTS. I-Haze, and O-Haze [44, 34, 45]

Potential Application: This algorithm can be used in surveillance, Military, underwater, outdoor image post-processing, and onboard moving vehicles to enhance visibility and clear vision.

Reference

[1] J Mao, Study of Image Dehazing with the self-adjustment of the Haze Degree, Ph.D. Thesis, Division of Production and Information

Systems Engineering, Muroran Institute of Technology, 2015

[2] H. Koschmieder, Theorie der horizontalensichtweite, Beitr.Phys. Freien Atm., vol. 12, 1924, pp. 171–181.

[3] S Roy, S S Chaudhuri, Modeling of Ill-Posed Inverse Problem, IJMECS, 2016, 12, pp-46-55

[4] K.,He, J., Sun, and X., Tang,: Single image haze removal using dark channel prior", IEEE Conference on Computer Vision and Pattern Recognition, Miami, FL, 2009, pp- 1956 – 1963

[5] R Tan, Visibility in Bad Weather from A Single Image, 2008CPVRIEEE Explore, DOI: 10.1109/CVPR.2008.4587643, ISSN: 1063-6919.

[6] Tarel, J.-P., Hautiere, N.: Fast visibility restoration from a single color or gray level image, IEEE 12th International conference on Computer Vision (2009) 2201 – 2208.

[7] R Fattal, Single Image Dehazing, ACM Transaction on Graphics(TOG), vol-27, Issue-3, August2008.

[8] D Berman, T Treibitz, S Avidan, Non-local Image Dehazing, CVPR2016.

[9] D Das, S Roy, S S Chaudhuri, Dehazing Technique based on Dark Channel Prior model with Sky Masking and its quantitative analysis, CIEC16, IEEE Explore, IEEE Conference ID: 36757, IEEE Xplore Compliant ISBN No.: 978-1-5090-0035-7, IEEE Xplore Compliant Part No.: CFP1697V-ART, 978-1-5090-0035- 7/16/$31.00©2016IEEE

[10] S Roy, S S Chaudhuri, Development of Real Time Visibility Enrichment Algorithms NCECERS2016

[11] S K Datta, M Hore, S Roy, Objective Evaluation of Dehazed Image by DCP, NCECERS2016-mainak

[12] S K Datta, M Hore, S Roy, Mathematical Modelling of Image Formation through Atmosphere, NSAMTM2016

[13] M Hore, S K Datta, S Roy, Subjective & Objective Evaluation of Dehazed Image by DCP, IC2C2SE2016

[14] D Roy, S Banerjee, S Roy, S S Chaudhuri, Removal of the Artifacts Present in the Existing Dehazing Techniques, IC2C2SE2016

[15] S Roy, S S Chaudhuri, Modelling and control of sky pixels in visibility improvement through CSA, IC2C2SE2016

[16] S Roy, S S Chaudhuri, Modeling of Haze Image as Ill posed Inverse Problem & its solution, IJMECS, vol:8, no:12, pp:46-55, December2016.

[17] I Pitas, A N Venetsanopoulos, Order Statistics in Digital Signal Processing, Proceedings of IEEE, Vol-80, No-12, December 1992.pp- 1893-1921.

[18] R C Gonzalez, R E Woods, Digital Image Processing, 3rd Edition, Pearson.

[19] N Hautiere, J P Tarel, D Aubert, E Doumont, Blind contrast enhancement assessment by gradient rationing at visible edges, Image Analysis and stereology.

[20] V Radhika, G Padmavati, Performance of various order statistics filters in impulse and mixed noise removal for RS images, Signal & Image Processing: An International Journal(SIPIJ) Vol.1, No.2, December 2010

[21] C Mythili, V Kavitha,Efficient technique for color image noise reduction, The Research Bulletin of Jordan ACM,Vol II(III)

[22] X Xhang, D H Brainard, Estimation of Saturated Pixel Values in Digital Colour Imaging, Optical Society of America, Vol-21, No-8,pp- 2301-2310.

[23] M Sipser, Introduction to the theory of computation, Cengage Learning.3rd Edition, 2013.

[24] I Stoganovic, P Stanimirovic, M Miladinovic, Applying the algorithm of Lagrange Multipliers in digital image restoration.

[25] T Chan, S Esedoglu, F Park, A Yip, Recent Trends in Total Variation Image Restoration, Mathematical Model in Computer Vision: A Hand Book, Department of Mathematics, University of Californis, 1-18, 2004.

[26] A Buades,B Coll, J M Morel, A Reviw of Image Denoising Algorithms, with a new one, ” Multiscale Model. Simul., vol. 4, no. 2, pp. 490–530, 2005.

[27] G Landi, Lagrangian Methods for the regularization of the discrete ill-posed problems, Computational Optimization and Applications, 39(3), 347-368, Springer US,2008.

[28] D Baraff,Linear Time Dynamics using Lagrange Multipliers, Carneigie Mellon University, 1996.

[29] M Subbarao, On the Depth Information in The Point Spread Function of a Defocused Optical System, State University of New York, 1999.

[30] E Pontelli, K Vellaverde, Complexity of Algorithms, Department of Computer Science,New Maxico State University.

[31] Sangita Roy, Sheli Sinha Chaudhuri, Low Complexity Single Colour Image Dehazing Technique, Intelligent Multidimensional Data and Image Processing,2018, IGI Global (formerly Idea Group Inc.).

[32] E J McCartney, Optics of the Atmosphere: Scattering by Molecules and Particles, New York, NY, USA:Wiley, 1976.

[33] Sangita Roy & Sheli Sinha Chaudhuri (2022) WLMS-based Transmission Refined Self-Adjusted No Reference Weather Independent Image Visibility Improvement, IETE Journal of Research, 68:3, 1635-1651, DOI: 10.1080/03772063.2019.1662335.

[34} C. O. Ancuti, C. Ancuti, R. Timofte and C. De Vleeschouwer, "O-HAZE: A Dehazing Benchmark with Real Hazy and Haze-Free Outdoor Images," 2018 IEEE/CVF Conference on Computer Vision and Pattern Recognition Workshops (CVPRW), Salt Lake City, UT, USA, 2018, pp. 867-8678, doi: 10.1109/CVPRW.2018.00119.

[35] M. Ju, C. Ding, C. A. Guo, W. Ren and D. Tao, "IDRLP: Image Dehazing Using Region Line Prior," in IEEE Transactions on Image Processing, vol. 30, pp. 9043-9057, 2021, doi: 10.1109/TIP.2021.3122088.

[36] R Fattal, Dehazing using color-lines. *ACM transactions on graphics (TOG)* 34.1 (2014): 1-14.

[37] L. K. Choi, J. You, and A. C. Bovik, “Referenceless prediction of perceptual fog density and perceptual image defogging,” *IEEE Trans. Image Process.*, vol. 24, no. 11, pp. 3888–3901, Nov. 2015.

[38] D. Berman, T. Treibitz, and S. Avidan, “Single image dehazing using haze-lines,” *IEEE Trans. Pattern Anal. Mach. Intell.*, vol. 42, no. 3, pp. 720–734, Mar. 2020.

[39] M. Ju, C. Ding, W. Ren, Y. Yang, D. Zhang, and Y. J. Guo, “IDE: Image dehazing and exposure using an enhanced atmospheric scat- tering model,” IEEE Trans. Image Process., vol. 30, pp. 2180–2192, 2021.

[40] W. Ren, S. Liu, H. Zhang, J. Pan, X. Cao, and M.-H. Yang, “Single image dehazing via multi-scale convolutional neural networks,” in Com- puter Vision—ECCV 2016, B. Leibe, J. Matas, N. Sebe, and M. Welling, Eds. Cham, Switzerland: Springer, 2016, pp. 154–169.

[41] D. Yang and J. Sun, “Proximal dehaze-net: A prior learning-based deep network for single image dehazing,” in Proc. Eur. Conf. Comput. Vis. (ECCV), 2018, pp. 702–717.

[42] Y. Qu, Y. Chen, J. Huang, and Y. Xie, “Enhanced Pix2pix dehazing network,” in Proc. IEEE/CVF Conf. Comput. Vis. Pattern Recognit. (CVPR), Jun. 2019, pp. 8152–8160.

[43] H. Dong et al., “Multi-scale boosted dehazing network with dense feature fusion,” in Proc. IEEE/CVF Conf. Comput. Vis. Pattern Recognit. (CVPR), Jun. 2020, pp. 2154–2164.

[44] B. Li et al., “Benchmarking single-image dehazing and beyond,” IEEE Trans. Image Process., vol. 28, no. 1, pp. 492–505, Jan. 2019.

[45] Ancuti, Cosmin, et al. "I-HAZE: a dehazing benchmark with real hazy and haze-free indoor images." Advanced Concepts for Intelligent Vision Systems: 19th International Conference, ACIVS 2018, Poitiers, France, September 24–27, 2018, Proceedings 19. Springer International Publishing, 2018.